PUBLICATION III

Systematic Design Approach for Capacitively Coupled Microelectromechanical Filters

In: IEEE Transactions on Ultrasonics, Ferroelectrics, and Frequency Control 2006. Vol. 53, No. 9, pp. 1662–1670.

Systematic Design Approach for Capacitively Coupled Microelectromechanical Filters

Ari T. Alastalo and Ville Kaajakari, *Member, IEEE*

***Abstract*—A design procedure for microelectromechanical (MEMS) band-pass filters is formulated that takes into account specifications set for carrier-to-interference ratio (C/I) and insertion loss. Since suppressing intermodulation distortion to maximize C/I in MEMS filter design typically leads to increased loss and vice versa, it is necessary to aim at a feasible compromise in filter performance that meets all of the requirements. In order to meet specifications that are typical for a handheld communication terminal, an integrated receiver architecture, where filter input and output impedances other than 50 Ω can be used, is found to be more feasible than resistively terminating the front-end filter at source and load to 50 Ω.**

I. Introduction

Communication systems operate in noisy environments where interferer powers may be 10^{10} times larger than the wanted-signal power. In order to ease the linearity and dynamic-range requirements of the receiver, high-quality-factor analog filters are used to block the interfering signals. Off-chip macroscopic ceramic surface acoustic wave (SAW) or film bulk acoustic resonator (FBAR) filters offer excellent performance but their large size, high cost, and unsuitability for integrated circuit (IC) integration limit their scope of application.

Miniature mechanical resonators, fabricated with microelectromechanical systems (MEMS) technology, are a potential replacement for off-chip filters as they are compact in size and integratable with IC electronics. The potential of miniature filters was already realized in the 1960s, leading to the development of the "resonant-gate transistor"—a field-effect transistor with a vibrating metal gate [1]. However, this early work was plagued by problems with a low quality factor (∼500 at 5 kHz), poor stability of the metal resonator, and limited dynamic range due to nonlinear electrostatic effects arising from the inverse gate capacitance-displacement relationship.

In the 1990s, the advances in processing technology and the tremendous growth of the communication-device market led to renewed interest in micromechanical resonators and filters [2]–[5]. The demonstrated quality factors of MEMS resonators, $Q > 100\,000$ at 10 MHz [6] and $Q > 1\,000$ at 1 GHz [7], are comparable to those of their macroscopic SAW and FBAR counterparts. While the mechanical properties of MEMS resonators now are very promising, the electrostatically coupled resonators characteristically suffer from high electrical impedance due to the weak electromechanical coupling. Increasing the coupling by reducing the electrode gap also increases the nonlinear electrostatic effects leading to trade-off between insertion loss and linearity [8].

In this paper, we quantify the trade-off in MEMS filter performance between the insertion loss and intermodulation distortion. Our prior analysis of filter distortion for the interferers at filter passband [9] and at stopband [10], [11] is summarized and a design procedure for MEMS bandpass filters is formulated in more general terms than in [11]. By means of advanced simulation tools, the analytical and experimental results on intermodulation in capacitively weakly coupled resonators are shown to also hold for higher-order filters as well as for tightly coupled filters. The central challenges for MEMS in high-frequency filter design are identified and exemplified by using the Global System for Mobile Communications (GSM) 900 specifications as a case study. Different filter architectures are compared and bandpass MEMS filters are shown to be more suitable for novel integrated receiver architectures than for the conventional resistive 50-Ω termination at filter input and output.

II. Theory of MEMS Filters

To facilitate practical filter design, the exact theory of MEMS filter distortion for single-stage weakly coupled filters, presented in [9], [10], is generalized to hold for tightly coupled and multi-stage filters. With simplifying assumptions, a set of easy-to-use design equations is derived.

A. Electrical Model

Fig. 1(a) shows a schematic of a MEMS resonator with spring coefficient k, effective mass m, resonance frequency $\omega_{\text{res}} = \sqrt{k/m}$, and dissipation $\gamma = \sqrt{km}/Q$, where Q is the unloaded quality factor of the resonator. The electrical transduction is provided by two capacitive transducers biased with DC voltage V_{bias}. The resonator is electrically grounded. Identifying the electromechanical coupling coefficient $\eta = C_0 V_{\text{bias}}/d$ and electromechanical spring constant $k_e \equiv \eta V_{\text{bias}}/d$, where C_0 is the rest capacitance of the electrostatic transducers and d is the transducer gap, the well-known electrical-equivalent model, shown in

Manuscript received October 13, 2005; accepted April 26, 2006. This work is supported by the Academy of Finland (grant 20542), Aplac® Solutions, VTI Technologies, Okmetic, and Tekes (National Technology Agency of Finland).

The authors are with VTT Technical Research Center of Finland, Tietotie 3, Espoo, FIN-02150, Finland (emails: ari.alastalo@vtt.fi, ville.kaajakari@vtt.fi).

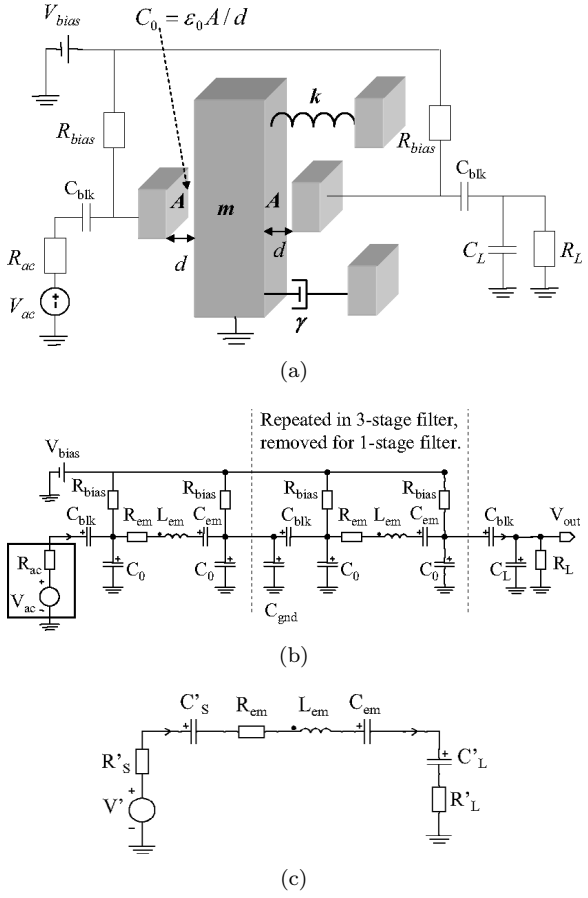

Fig. 1. MEMS resonator and filter models. The DC-blocking capacitance is denoted $C_{\rm blk}$. The electrical equivalent of the resonator in (a) is the RLC series-resonance circuit ($R_{\rm em}$, $L_{\rm em}$, $C_{\rm em}$) with the two shunt capacitors C_0 in (b). Close to the resonance frequency, the single-stage filter has a series equivalent shown in (c). (a) Schematic of a micromechanical resonator (k, m, γ) operating as a single-stage band-pass filter for capacitively coupled signals. (b) Electrical equivalent of a single-stage (a) and multi-stage MEMS filters. Coupling of the filter stages is done with a shunt capacitance $C_{\rm gnd}$. (c) Series equivalent of the single-stage filter.

Fig. 1(b) [3], [4], [12], can be developed. Here, $R_{\rm em} = \gamma/\eta^2$, $L_{\rm em} = m/\eta^2$ and $C_{\rm em} = \eta^2/(k - 2k_e)$ are the resistance-inductance-capacitance (RLC)-equivalent parameters of the MEMS resonator. The inter-stage coupling is represented with a shunt capacitance $C_{\rm gnd}$ but it may be either a physical capacitance or a mechanical spring.

For the single-resonator filter, the loaded in-circuit quality factor Q' can be calculated as

$$Q' = \sqrt{k'm}/\gamma'. \tag{1}$$

Here,

$$\gamma' = \eta^2 \left(R_{\rm em} + R'_S + R'_L\right), \tag{2}$$

$$k' = \eta^2 \left(1/C_{\rm em} + 1/C'_S + 1/C'_L\right), \tag{3}$$

where R'_S, C'_S, R'_L, and C'_L are the narrow-band series-equivalent resistances and capacitances of the parallel source ($R_{\rm ac}||C_0$) and load ($R_L||(C_0+C_L)$) circuits, respectively, given by

$$R'_S = \frac{R_{\rm ac}}{(R_{\rm ac}\omega_0 C_0)^2 + 1}, \tag{4}$$

$$C'_S = \frac{C_0\left[(R_{\rm ac}\omega_0 C_0)^2 + 1\right]}{(R_{\rm ac}\omega_0 C_0)^2}, \tag{5}$$

$$R'_L = \frac{R_L}{\left[R_L\omega_0(C_0 + C_L)\right]^2 + 1}, \tag{6}$$

$$C'_L = \frac{(C_0 + C_L)\left\{\left[R_L\omega_0(C_0 + C_L)\right]^2 + 1\right\}}{\left[R_L\omega_0(C_0 + C_L)\right]^2}, \tag{7}$$

and $\omega_0 = \omega' \equiv \sqrt{k'/m}$ is the loaded resonance frequency. In addition to the loaded Q value of (1), the Thévenin-equivalent input voltage

$$V'_{\rm ac} = V_{\rm ac}\frac{1}{1 + j\omega C_0 R_{\rm ac}} \tag{8}$$

must be used in order to utilize the unloaded third-order input intercept point (IIP3) and signal-to-intermodulation ratio (SIR) results of [9] and [10] for tightly coupled filters, as in what follows.

B. Intermodulation

In filter applications, signal intermodulation (IM) due to odd-order nonlinearities is especially detrimental as it can lead to unwanted frequency components within the filter passband. For example, cubic mixing of two fundamental signals having frequencies ω_1 and ω_2 results in third-order intermodulation (IM3) products at frequencies $2\omega_1 - \omega_2$ and $2\omega_2 - \omega_1$. If $\omega_1 = \omega_0 + \Delta\omega$ and $\omega_2 = \omega_0 + 2\Delta\omega$, the IM product at $2\omega_1 - \omega_2$ is at the passband center frequency ω_0, corrupting the desired signal.

The SIR in the output of a capacitively coupled MEMS single-resonator filter for interferers outside the passband is given in [10] for a general case. For present purposes, we assume that: 1) the passband desired-signal frequency ω_0 is much higher than the frequency separation $\Delta\omega$ to the interferers present in the filter input at frequencies $\omega_1 = \omega_0 + \Delta\omega$ and $\omega_2 = \omega_0 + 2\Delta\omega$; 2) the bias voltage is much lower than the electromechanical pull-in voltage at which bias level the resonator becomes unstable; and 3) mechanical nonlinearities in the spring k of Fig. 1(a) can be ignored as much weaker than the capacitive transducer nonlinearities. With these assumptions, (23) of [10] simplifies as

$$\mathrm{SIR} = \frac{8\,|\Delta\omega|\,\omega_0\,V_{\rm bias}^2\sqrt{P_{\rm sig}}}{5\,\omega_e^2\,R'_S\,P_{\rm int}\sqrt{P_{\rm int}}}, \tag{9}$$

where $\omega_e \equiv \sqrt{k_e/m}$. It is convenient to use (9) for filter design instead of the general solution of [10] because (9) can be solved for the gap d in the closed form (ω_e and R'_S are functions of d). The AC-source powers (see Fig. 1) for the signal and interference are $P_{\rm sig} = V_{\rm ac,sig}^2/(2R_{\rm ac})$ and

$P_{\rm int} = V_{\rm ac,int}^2/(2R_{\rm ac})$, respectively. The AC power corresponding to the IIP3 is related to the SIR as

$$P_{\rm IIP} = {\rm SIR}\sqrt{\frac{P_{\rm int}^3}{P_{\rm sig}}}. \quad (10)$$

When the interferers are inside the passband, we have [9]

$$P_{\rm IIP}^{\rm IB} = \frac{V_{\rm bias}^2}{R_S'\sqrt{(6q^3+q/2)^2+9q^4}}, \quad (11)$$

where $q \equiv Q'\,\omega_e^2/\omega_0^2 = Q'\,k_e/k'$.

C. Insertion Loss

The passband voltage gain is

$$G_V = \frac{V_{\rm out}}{V_{\rm ac}/2} = \frac{2}{\omega_0 C_L'(R_S'+nR_{\rm em}+R_L')}\frac{|1+j\omega_0 C_L' R_L'|}{|1+j\omega_0 C_0 R_{\rm ac}|}, \quad (12)$$

where n is the filter order and R_S', $R_{\rm em}$, R_L', $R_{\rm ac}$, C_L', C_0, $V_{\rm ac}$, and $V_{\rm out}$ are as shown in Fig. 1. We note that with a dominantly capacitive termination ($|1/\omega_0 C_L'| > R_L'$) it is possible to obtain voltage gain because the filter acts as an RLC impedance transformer.

III. Model Verification

The validity of the analytical SIR model has been verified by harmonic-balance Aplac® circuit simulations [13], [14] and experiments for single-stage filters [9], [10]. In what follows, simulations with one-, two-, and three-stage filters are performed to show that the analytical SIR model can also be applied for higher-order filters as well. Moreover, by analyzing 1-GHz MEMS filters and comparing their performance to GSM specifications, it is shown that the simplified expressions (9) and (11) suffice to estimate the linearity properties of MEMS filters.

A. 13-MHz Band-Pass Filters

We consider the one-, two-, and three-stage filters of Fig. 1 with the 13-MHz bulk acoustic wave (BAW) MEMS resonators of [10] where $Q = 47000$ but with a reduced gap of 25.5 nm in order to have a low mechanical impedance of 38 Ω. The other relevant resonator parameters are summarized in Table I. We use $C_{\rm gnd} = 20$ pF and $C_{\rm gnd} = 30$ pF for the two-stage and three-stage filters, respectively. Furthermore, we use a resistive termination with $C_L = 0$ and $R_L = R_{\rm ac}$ in Fig. 1. What is not included is a parasitic feed-through capacitance between input and output that would reduce the stopband attenuation of the filters but would not affect the intermodulation properties.

Fig. 2 shows simulated responses of the filters with 2 Ω (unloaded, $R_{\rm ac} \ll R_{\rm em}$) and 450 Ω (loaded, $R_{\rm ac} \gg R_{\rm em}$) source and load impedances. The 450-Ω source and load yields $Q' = 1900$ for the in-circuit quality factor (1) of the resonator. The unloaded case is not useful as a filter due to the large insertion loss and ripple in the passband. The loaded cases demonstrate that, with increasing filter order, the stopband slope steepens but the insertion loss increases also due to the increasing series resistance at resonance.

TABLE I
Parameters for the BAW Resonator.

k	16.3 MN/m	$f_{\rm res}$	13 MHz	Q	47000
d	25.5 nm	C_0	2 pF	$U_{\rm pi}$	38 V
$V_{\rm bias}$	3.8 V	η	335 μFV/m	k_e	51 kN/m
$R_{\rm em}$	38 Ω	$L_{\rm em}$	22 mH	$C_{\rm em}$	7 fF

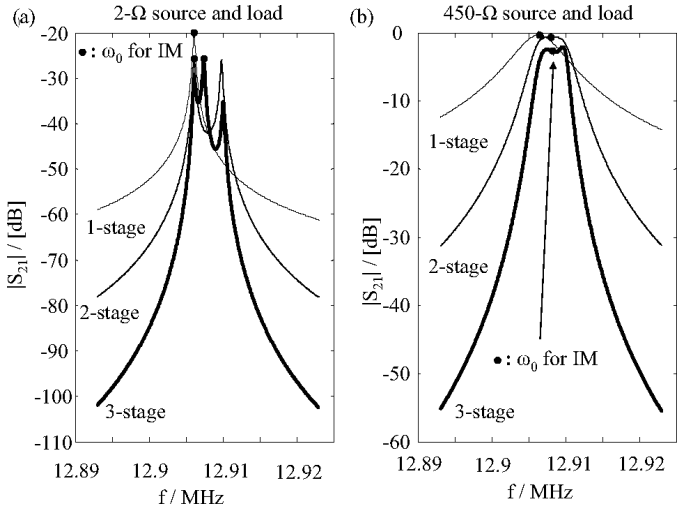

Fig. 2. Unloaded (a) and loaded (b) responses of the filters composed of one, two, and three BAW resonators, as shown in Fig. 1. The desired-user frequency ω_0 for the SIR results of Fig. 3 is marked with a dot.

Fig. 3 shows the analytic and simulated SIR for the filters with ω_0 as indicated in Fig. 2. A different choice for ω_0 within the passband would be equally justified. The analytic results, calculated with the exact formulas of [10] for the single-stage filter, are in excellent agreement with the simulations. Moreover, for out-of-band interferers with $\Delta\omega \to \infty$, the approximate expression (9) (marked as approximation in Fig. 3) becomes valid. It is seen that outside the passband the unloaded single-resonator result is also valid for the higher-order filters as well as for the tightly coupled filters provided that the loaded quality factor of (1) and the Thévenin-equivalent input voltage of (8) are used. Intuitively, this is to be expected because for the out-of-band interferer frequencies, the resonator impedances are high and the resonators are therefore only weakly coupled. Thus, the first resonator and the first transducer effectively set the SIR. At some frequencies close to the passband edge, the numerical harmonic-balance simulation does not converge for the unloaded two-stage and three-stage filters. This is seen in the discontinuities of the corresponding curves of Fig. 3 with $R_{\rm ac} = 2$ Ω.

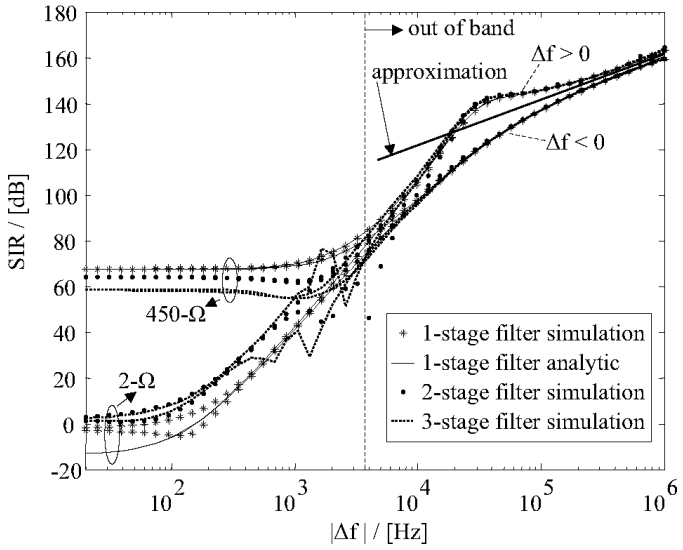

(a)

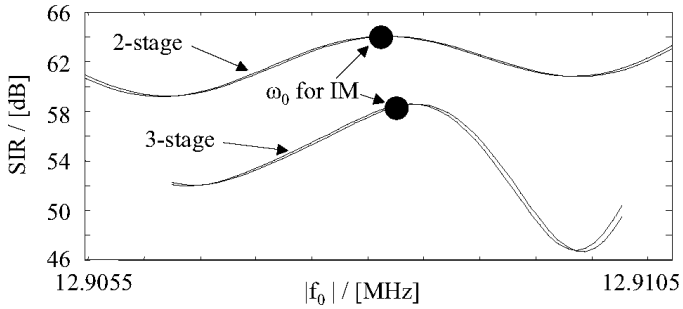

(b)

Fig. 3. Signal-to-intermodulation ratio as a function of the interferer frequency separation $\Delta f = \Delta\omega/(2\pi)$ for the filters of Fig. 2. (a) SIR as a function of Δf for the filters of Fig. 2 with a −20 dBmV desired signal at ω_0, marked with a dot in (b) and in Fig. 2, and with 0 dBmV interferers. The result given by (9), used in this paper for filter design, is marked approximation. (b) In-band SIR for the loaded two-stage and three-stage filters in (a) with $\Delta f = 20$ Hz and with the signal frequency $f_0 = \omega_0/(2\pi)$ swept across the passband.

For the single-stage filters in Fig. 3, the in-band approximation (11) approaches the exact results as $\Delta\omega \to 0$. Namely, (11) and (10) give SIR = −13.4 dB (IIP3 = 3.3 dBmV) and SIR = 67 dB (IIP3 = 43.5 dBmV) for the unloaded and loaded single-stage filters, respectively. The higher source and load resistances result in a lower loaded quality factor of the filter and thus a higher SIR. The deviation of the analytical estimate from the simulated results for the unloaded filter, when $\Delta f \to 0$, is understood since the interferer voltage of 0 dBmV is of the same order as the IIP3 input voltage of 3.3 dBmV. Consequently, for such strong interferers, harmonics higher than third order, that are not taken into account in theory, become important and reduce the gain for the IM3 products.

For the higher-order filters, the in-band SIR is seen to depend on the chosen ω_0 within the passband as demonstrated in Fig. 3(b). This is expected because the S_{21} also has ripples as the coupled resonators move in and out of phase. However, the single-stage approximation is still shown to be a good order-of-magnitude estimation.

TABLE II
PARAMETERS FOR THE 1-GHZ FILTER CONFIGURATIONS.*

	A	B	C	Units
V_{bias}	40	**147**	**16**	V
d	30	30	**10**	nm
ω_e	152	560	316	10^6 rad/s
R_{ac}	1000	50	50	Ω
R'_S	690	49.9	49.5	Ω
R_{em}	663	49	51	Ω
C_0	93	93	278	fF
Q'	2500	2500	2600	
f'	1.149	1.143	1.148	GHz
G_V	−16	8.3	6.7	dB

*(A) The theoretical resonator of [7]; (B) same as (A) but scaled to $R_{\text{em}} \approx 50$ Ω by increasing the bias voltage; (C) same as (A) but scaled to $R_{\text{em}} \approx 50$ Ω by reducing the gap.

TABLE III
SIR FOR THE RESONATORS OF TABLE II USED AS A FILTER FOR GSM 900.*

GSM 900		resulting SIR			
Δf	P_{int}	A	B	C	
−10	0	**−2**	**14**	**−10**	outside GSM-RX band
−3	−23	55	63	44	
−0.6	−43	96	87	76	
0.6	−43	111	90	85	
3	−23	59	77	58	
10	0	**−1**	**28**	**−5**	outside GSM-RX band
± 10	0	**−2**	**21**	**−8**	(9)
MHz	dBm	dB	dB	dB	

*The approximation (9) gives a good estimate for $|\Delta f| = 10$ MHz. The signal power ($P_{\text{sig}} = -99$ dBm) and the interferer powers (P_{int}) are as specified in [15].

B. 1-GHz Single-Stage Filters

As another example, we consider 1-GHz single-stage filters based on the resonators of [7] with $k = 373.1$ MN/m, $f_{\text{res}} = 1.150$ GHz, and $Q = 5100$. The load of the filter is now taken to be an FET amplifier stage with $R_L = 1$ MΩ and $C_L = 1$ pF in Fig. 1. This does not reduce the in-circuit Q value (1) as much as the resistive termination at both sides of the filter. Furthermore, by effectively tapping the mechanical RLC resonator, voltage gain becomes attainable, enabling the use of resonators with $R_{\text{em}} \sim 1$ kΩ without introducing significant signal attenuation. The filter input is thought to be directly connected to an antenna, where different impedances can be realized, but the different impedance levels can also be realized with a transformer. For a given impedance level, the source voltage V_{ac} is calculated from the source power level.

Table II shows relevant parameters for three different filter configurations where (A) is based on the resonator of [7] whereas for (B) and (C) the mechanical impedance is reduced to $R_{\text{em}} \approx 50$ Ω by changing the bias voltage and the gap. Table III shows the resulting SIR when the filters (A), (B), and (C) of Table II are used as a front-end filter for GSM 900. As the filter passband is narrower here than

the GSM-RX band, one would need a multitude of such filters with different center frequencies to cover all of the channels. The filters could be connected in parallel or a switch could be used to select only one of the filters, corresponding to a particular channel, to be used at a time. The signal and interference powers in Table III are as specified for a desired signal and for blockers in [15]. Furthermore, we assume two blockers of equal amplitude at frequencies $f_0+\Delta f$ and $f_0+2\Delta f$ to interfere with the desired signal at f_0. The same SIR is found in simulations and with the theory of [10]. The approximation (9) gives a good estimate for $|\Delta f| = 10$ MHz. It is seen that two 0-dBm interferers at 10-MHz and 20-MHz separation from the desired signal reduce the SIR below acceptable levels except for filter (B) for which the bias voltage is not feasible at least in portable devices. For these interferers, marked as outside GSM-RX band in Table III, the desired-user frequency is taken to be at the edge of the GSM-RX band.

As the results in Table III clearly show, the hardest linearity requirements are set by the 0-dBm out-of-GSM-RX-band interferers at 10 MHz and 20 MHz off the desired-signal frequency[1]. As the SIR for the other interferers is easily sufficient, it is enough to use the simplified expression (9) as a starting point for filter design. Moreover, successful filter design is not trivial and a systematic design approach is needed. This is developed in Section IV.

IV. Filter Design

In what follows, we derive design criteria for the resonator dimensions, transducer gap, Q value, and bias voltage from specified in-band and out-of-band filter attenuation and maximum distortion. The criteria yield a systematic procedure to design MEMS filters for communication applications.

A. Out-of-Band Attenuation

For minimum performance, the filter should suppress the interferers situated outside the systems reception (RX) band to the same level as the strongest interferers within the RX band. If this is achieved, the linearity requirement for the low noise amplifier (LNA) and mixer are set by the in-band interferers that normally are not affected by band-select filtering. Denoting the minimum attenuation at frequency f with respect to the desired-signal frequency f_0 (selectivity) as $A_{\min}$, the minimum required in-circuit Q' value in (1) can be derived. For the single-stage MEMS filter, this leads to

$$Q' \geq \frac{\sqrt{A_{\min}^2 - (f/f_0)^2}}{\left|1-(f/f_0)^2\right|} \equiv Q'_{\min}. \tag{13}$$

[1]The intermodulation performance for out-of-band blockers is not clearly defined in the GSM specifications. However, the out-of-band intermodulation is known to set the strongest linearity requirements in code division multiple access (CDMA) design [16]. The out-of-band intermodulation is therefore considered also for GSM.

Increasing the filter order makes the stopband response a steeper function of frequency, and thus a lower quality factor for the resonators is sufficient at the cost of a higher insertion loss.

B. Out-of-Band Intermodulation

The weakest signal, with power P_{sig}, to be detected in the presence of interferers, having powers P_{int}, at $f_0+\Delta f$ and $f_0+2\Delta f$ leads to requirements for intermodulation performance. Typically, this is specified with the minimum SIR ($\text{SIR}_{\min}$) that the filter needs to satisfy in its output in order to meet the overall system carrier-to-interference (C/I) ratio target. Requiring that the SIR be greater than or equal to the minimum $\text{SIR}_{\min}$ gives from (9)

$$d^3 + (\epsilon_0 A\omega_0 R_{\text{ac}})^2 d \geq \frac{\epsilon_0 A R_{\text{ac}}}{m}\frac{5P_{\text{int}}\sqrt{P_{\text{int}}}\text{SIR}_{\min}}{8|\Delta\omega|\omega_0\sqrt{P_{\text{sig}}}}, \tag{14}$$

which is also valid for higher-order filters as shown in Section II. Result (14) is easily derived after noting that both ω_e and R'_S in (9) are functions of the gap. If $R'_S \approx R_{\text{ac}} \Leftrightarrow (R_{\text{ac}}\omega_0 C_0)^2 \ll 1$, (14) simplifies to

$$d \geq \left(\frac{\epsilon_0 A R_{\text{ac}}}{m}\frac{5P_{\text{int}}\sqrt{P_{\text{int}}}\text{SIR}_{\min}}{8|\Delta\omega|\omega_0\sqrt{P_{\text{sig}}}}\right)^{1/3}. \tag{15}$$

Eq. (14) and (15) show that to meet the performance requirements given as $\text{SIR}_{\min}$, there is a minimum for the gap.

C. In-Band Loss

Requiring that the passband voltage gain G_V, given by (12), be greater than a minimum gain $G_{\min}$, set by the insertion loss specifications, gives

$$QV_{\text{bias}}^2 \geq \frac{nd^4\sqrt{km}}{(\epsilon_0 A)^2\left\{\frac{2}{\omega_0 C'_L G_{\min}}\frac{|1+j\omega_0 C'_L R'_L|}{|1+j\omega_0 C_0 R_{\text{ac}}|} - R'_S - R'_L\right\}}. \tag{16}$$

Thus, once the gap d is chosen, the unloaded quality factor Q and the bias voltage V_{bias} need to be chosen to meet the insertion loss specifications. As the unloaded quality factor is usually determined by material properties, effectively this gives a requirement for the bias voltage.

D. In-Band Intermodulation

The in-band intermodulation is estimated from (11) by considering 1) the signal self distortion, and 2) in-band interferers. However, typically the out-of-band interferers give more stringent linearity requirements. Therefore, after choosing the filter parameters, it is usually sufficient to check that the filter meets the in-band specifications. If these are not met, then the filter gap should be increased and the design adjusted accordingly.

TABLE IV
SIMPLIFIED FILTER REQUIREMENTS FOR GSM 900 [15].

Specification		Comment
$\mathrm{SIR}_{\min}$	9 dB	(9) ⇒ (14), full rate speech
$G_{\min}$	−3 dB	(12) ⇒ (16), in-band loss
$A_{\min}(f - f_0 = 10\ \mathrm{MHz})$	23 dB	(13), minimum selectivity
to be met with :		
P_{sig}	−99 dBm	Signal
$P_{\mathrm{int}}(\Delta f = 0\ \mathrm{Hz})$	−49 dBm	In-band interferer
$P_{\mathrm{int}}(\Delta f = 10\ \mathrm{MHz})$	0 dBm	Out-of-band interferer

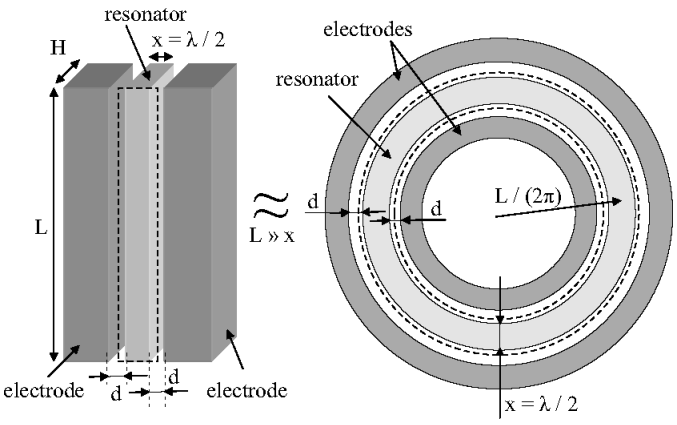

Fig. 4. Test geometry for resonator design showing the resonator surrounded by the electrodes. The dotted line indicates the vibration mode shape in the extended state.

V. GSM 900 Filter Design Example

In the following, the usage of the design equations of Section IV is illustrated by a single-stage MEMS front-end filter design for $f_0 = 1$ GHz with the requirements of the GSM 900 mobile device. The simplified requirements are shown in Table IV. These specifications should be considered as exemplary performance requirements and a realistic system design may set more or less stringent goals.

A. Resonator Geometry

Let us now, as a simple example, consider a bar geometry shown in Fig. 4. The resonating dimension is $x = \lambda/2 = v/(2f_0) \approx 4\ \mu$m for $f_0 = 1$ GHz. Here $v = \sqrt{Y/\rho}$ is the bulk acoustic wave velocity with $\rho = 2330\ \mathrm{kg/m^3}$ the density and $Y = 168$ GPa the Young's modulus of silicon. This simple geometry can also approximate the ring geometry [17], shown at the right-hand side of Fig. 4, when the ring radius $L/(2\pi)$ is much larger than the ring width x. The capacitive transducers at both sides of the resonator have an area of $A = HL$ and rest capacitance of $C_0 = \epsilon_0 HL/d$, where d is the gap. The effective mass and spring coefficient are now [18]

$$m = \rho L x H/2, \tag{17}$$

$$k = \pi^2 Y L H/(2x). \tag{18}$$

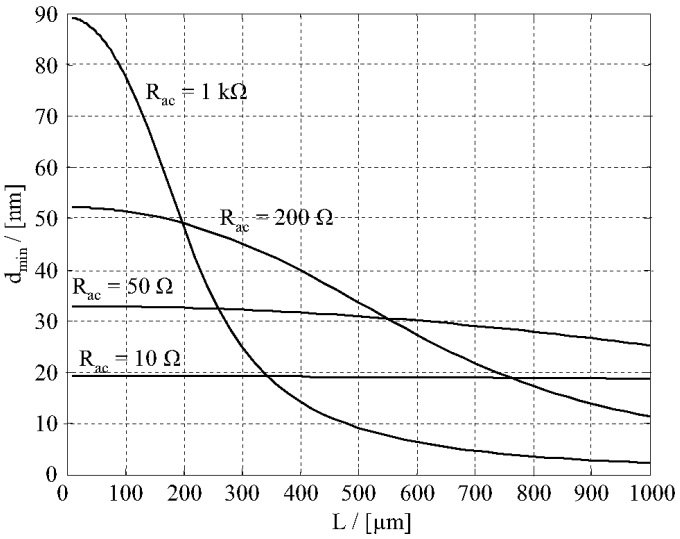

Fig. 5. Minimum gap (14), determined by the maximum out-of-band intermodulation, for the resonators of Fig. 4 with $H = 10\ \mu$m.

B. Minimum Quality Factor

From the minimum interference attenuation requirements in Table IV, one obtains (13) $Q' = 700$ for the minimum loaded quality factor. For channel-select filtering, the passband is 200 kHz, corresponding to a much higher in-circuit quality factor of $Q' = 5000$, which would also be enough for $A_{\min} = 40$ dB at 10 MHz off the passband in (13), as typically satisfied by commercial FBAR filters.

C. Minimum Gap (Linearity)

Given the resonator geometry, the minimum gap $d_{\min}$ is solved from (14). Fig. 5 shows the minimum gap for $R_{\mathrm{ac}} \in \{10, 50, 200, 1000\}\ \Omega$ as a function of the transducer length L with $H = 10\ \mu$m. For small L, (15) is a good approximation and gives, for example, $d_{\min} = 19$ nm and $d_{\min} = 33$ nm for $R_{\mathrm{ac}} = 10\ \Omega$ and $R_{\mathrm{ac}} = 50\ \Omega$, respectively. With increasing L, the effect of increasing C_0 requires the use of (14). As Fig. 5 illustrates, the minimum gap $d_{\min}$ increases with increasing source impedance R_{ac}. This is due to increase in source voltage level V_{ac} for given source power.

D. Minimum QV_{bias}^2 (Insertion Loss)

We now set the gap close to its minimum value for the resonators of Fig. 5, say, $d(L) = d_{\min} + 3$ nm, after which C_0 and the other needed parameters are determined in order to calculate the minimum value for QV_{bias}^2 in (16). In what follows, two architectures are considered: 1) the conventional resistive termination, and 2) an integrated filter where the filter output is directly connected to a capacitive FET LNA load while the filter input is fed from a resistive source such as an antenna.

Fig. 6 shows the calculated minimum QV_{bias}^2 for three different loads: a resistive load and two different capacitive

loads. Note that in Fig. 6, the $d(L) = d_{\min} + 3$ depends on the resonator length L and is obtained from Fig. 5. The central challenge in MEMS filter design for portable low-voltage devices, namely, very high QV_{bias}^2, is clearly illustrated. To calculate the actual filter parameters, we assume $Q = 5000$ and $H = 10$ μm. Table V summarizes the selected filter designs that are indicated in Fig. 6 with circles and labels (A) and (B). All designs of Table V, except the one with a 1-kΩ resistive load, satisfy the requirements in Table IV. For the resistive 1-kΩ load, the loaded quality factor is too low for (9) to be a good approximation for the SIR. A solution would be to correct the design by requiring a somewhat higher $\text{SIR}_{\min}$. It is also seen that with the resistive load quite a large resonator size and a small electrode gap are needed.

As is evident from (12), terminating the resonator with a capacitive load enables voltage gain as the resonator RLC circuit is effectively tapped. Consequently, a capacitive load of $C_L = 1$ pF corresponding to a typical LNA FET input, would allow a more realistic filter size. With an even higher load impedance of $C_L = 0.1$ pF, the filter could be realized at $V_{\text{bias}} < 5$ V.

In Fig. 6, it was assumed for the gap that $d = d_{\min} + 3$ nm corresponding to the minimum gap $d_{\min}$ of Fig. 5. If the minimum achievable gap is determined by the fabrication process, Figs. 7 and 8 may be used to determine the minimum QV_{bias}^2 for capacitive and resistive loads, respectively. It is seen that for a fixed gap, there is an optimal resonator size resulting in the lowest QV_{bias}^2. For a capacitive load (see Fig. 7), a smaller source impedance R_{ac} results in smaller QV_{bias}^2 as larger impedances load the resonator more and thus reduce the attainable voltage gain from the resonator. The opposite holds for resistively terminated resonators as shown in Fig. 8. That is, for a resistive load with fixed gap, the source and load impedances should be large in comparison to R_{em} to minimize the insertion loss.

E. In-Band Linearity Check

For the in-band interference with $P_{\text{int}} = -49$ dBm [15] and a signal with $P_{\text{sig}} = -99$ dBm, (10) with a minimum SIR of 9 dB gives the requirement of

$$P_{\text{IIP}}^{\text{IB}} \geq -19.5 \text{ dBm} \equiv P_{\text{IIP,min}}^{\text{IB}}, \tag{19}$$

where $P_{\text{IIP}}^{\text{IB}}$ is given by (11). As shown in Table V, all designs satisfy the in-band linearity requirement.

VI. Conclusions

In this paper, the capacitive MEMS filter design was analyzed and the trade-off between linearity and insertion loss was qualified. For simplicity, a single-stage filter was considered and it was assumed that several filters would be in parallel to cover the entire RX band. For GSM, this would require more than ten filters which may be impractical. However, as the SIR analysis was shown to be valid

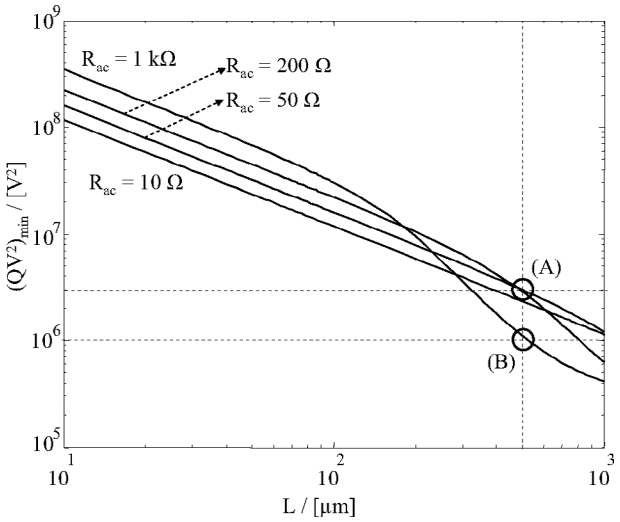

(a)

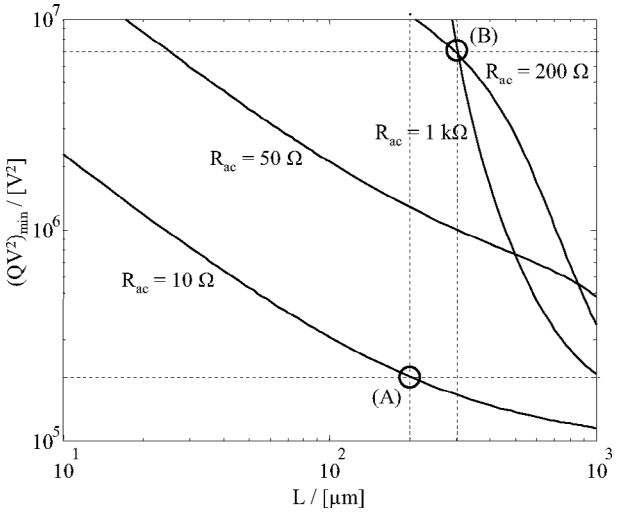

(b)

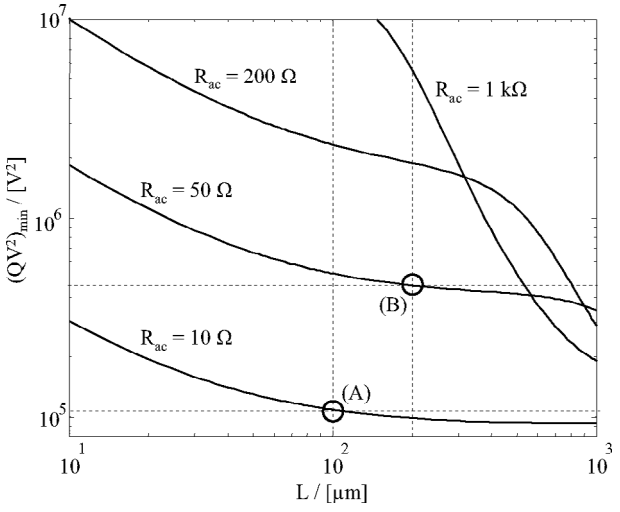

(c)

Fig. 6. Minimums of QV_{bias}^2 (16), determined by the maximum in-band loss of the filter, corresponding to the resonator geometries of Fig. 5 with $d(L) = d_{\min} + 3$ nm. The circles labeled (A) and (B) correspond to the designs of Table V. (a) Resistive load ($C_L = 0$, $R_L = R_{\text{ac}}$); (b) capacitive load ($C_L = 1$ pF, $R_L = 1$ MΩ); (c) capacitive load ($C_L = 0.1$ pF, $R_L = 1$ MΩ).

TABLE V
GSM 900 FILTER DESIGNS* INDICATED WITH CIRCLES IN FIG. 6.

Load impedance in Fig. 6	Selected case in Fig. 6	R_{ac} [Ω]	L [μm]	d [nm]	V_{bias} [V]	R_{em} [Ω]	Q' Eq. (1)	SIR Eq. (9) [dB]	SIR [10] $\Delta f < 0$ [dB]	SIR [10] $\Delta f < 0$ [dB]	P_{IIP}^{IB} Eq. (11) [dBm]	G_V Eq. (12) [dB]
Resistive load	(A)	200	500	37	24	52	1500	10	11	9.7	34	−3
Fig. 6(a)	(B)	1k	500	12	15	1.5	1400	11	17	5.6	15	−2.9
Capacitive load	(A)	10	200	22	**6.4**	230	4800	13	13	12	30	−2.6
1 pF, Fig. 6(b)	(B)	200	300	48	37	102	2200	10	11	9.6	29	−3
Capacitive load	(A)	10	100	22	**4.7**	841	4900	13	13	12	33	−2.6
0.1 pF, Fig. 6(c)	(B)	50	200	36	9.8	690	4700	12	12	11	33	−2.9

*In all designs $H = 10$ μm and $Q = 5000$.

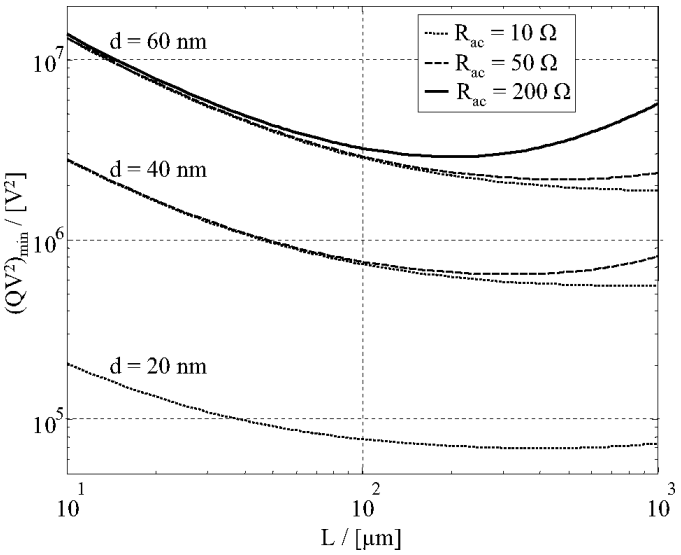

Fig. 7. Minimum of QV_{bias}^2, for a filter with capacitive load (C_L = 0.1 pF, $R_L = 1$ MΩ), and fixed gap sizes of $d \in \{20, 40, 60\}$ nm.

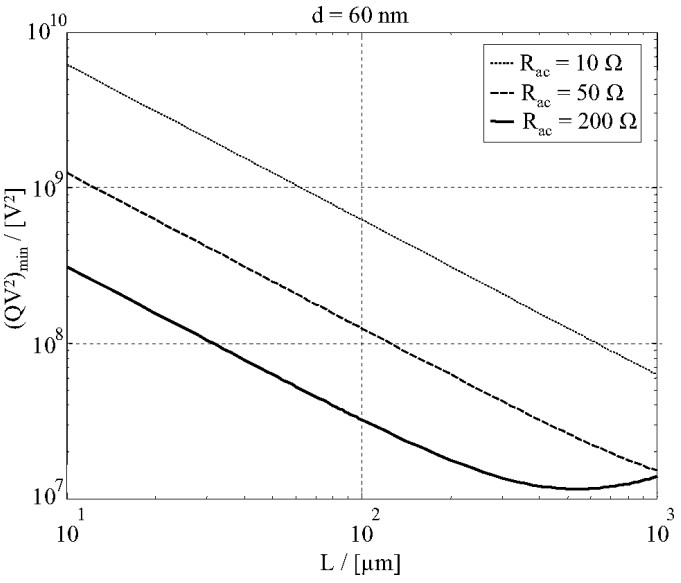

Fig. 8. Minimum of QV_{bias}^2, for a filter resistive load ($R_L = R_{ac}$) and a fixed gap size of $d = 60$ nm.

also for multi-stage filters, the conclusions also hold for higher-order pass-band filter designs. What is different for higher-order filters is that the losses in each stage add up and, consequently, the motional resistance has to be even lower than for the single-stage designs.

After the analysis, a systematic procedure to design MEMS band-pass filters was formulated. It was found desirable to utilize the high resonator quality factor for voltage gain that is enabled by capacitive load termination at the output of the filter. This is possible in integrated receiver architectures, where 50-Ω transmission lines are not needed between the antenna and the filter and between the filter and the LNA.

Using dielectric other than air/vacuum for the electrode gap has potential in lowering the electrical impedance, thus alleviating the need for a very narrow gap [19]. The analysis procedure derived in this paper can be directly applied for such devices as long as an appropriate value for permittivity is used.

The analysis in this paper was mainly theoretical and only few references were made to manufacturing where several challenges remain: 1) The gap should be reduced below 30 nm to enable bias voltages of the order of 5 V; 2) The dimensional tolerances of the filters, manufactured with lithography, are poor, leading to wide variations in center frequency; 3) The parasitic feed through capacitance may limit the filtering performance, and differential readout may be required. If these challenges are addressed, MEMS filters can have a large economic potential.

REFERENCES

[1] H. C. Nathansona, W. E. Newell, R. A. Wickstrom, and J. R. Davis, "The resonant gate transistor," *IEEE Trans. Electron Devices*, vol. 14, no. 2, pp. 117–133, Mar. 1967.

[2] C. T.-C. Nguyen and R. T. Howe, "CMOS micromechanical resonator oscillator," in *Tech. Dig. IEEE Int. Electron Devices Meeting*, Washington, DC, 5–8 Dec. 1993, pp. 199–202.

[3] H. Tilmans, "Equivalent circuit representation of electromechanical transducers: I. Lumped-parameter systems," *J. Micromech. Microeng.*, vol. 6, no. 1, pp. 157–176, Mar. 1996.

[4] L. Lin, R. T. Howe, and A. P. Pisano, "Microelectromechanical filters for signal processing," *J. Microelectromech. Syst.*, vol. 7, no. 3, pp. 286–294, Sep. 1998.

[5] C. T.-C. Nguyen, "Frequency-selective MEMS for miniaturized low-power communication devices," *IEEE Trans. Microwave Theory Tech.*, vol. 47, no. 8, pp. 1486–1503, Aug. 1999.

[6] V. Kaajakari, T. Mattila, A. Oja, J. Kiihamäki, and H. Seppä, "Square-extensional mode single-crystal silicon micromechanical resonator for low phase noise oscillator applications," *IEEE Electron Device Lett.*, vol. 25, no. 4, pp. 173–175, Apr. 2004.

[7] J. Wang, Z. Ren, and C. T.-C. Nguyen, "1.156-GHz self-aligned vinrating micromechanical disk resonator," *IEEE Trans. Ultrason., Ferroelect., Freq. Contr.*, vol. 51, no. 12, pp. 1607–1628, Dec. 2004.

[8] R. Navid, J. R. Clark, M. Demirci, and C. T.-C. Nguyen, "Third-order intermodulation distortion in capacitively-driven cc-beam micromechanical resonators," in *Tech. Dig. Int. IEEE Microelectromechanical Syst. Conf.*, Interlaken, Switzerland, 21–25 Jan. 2001, pp. 228–231.

[9] A. T. Alastalo and V. Kaajakari, "Intermodulation in capacitively coupled microelectromechanical filters," *IEEE Electron Device Lett.*, vol. 26, no. 5, pp. 289–291, May 2005.

[10] A. T. Alastalo and V. Kaajakari, "Third-order intermodulation in microelectromechanical filters coupled with capacitive transducers," *J. Microelectromech. Syst.*, vol. 15, no. 1, pp. 141–148, Feb. 2005.

[11] A. T. Alastalo and V. Kaajakari, "Designing capacitively coupled microelectromechanical filters," in *Proc. IEEE Ultrason. Symp.*, Rotterdam, The Netherlands, 18–21 Sep. 2005, pp. 1588–1591.

[12] S. Pourkamali and F. Ayazi, "Electrically coupled MEMS bandpass filters: Part I: With coupling element," *Sens. Actuators A*, vol. 122, no. 2, pp. 307–316, Aug. 2005.

[13] Aplac RF Design Tool, APLAC An AWR Company, www.aplac.com.

[14] T. Veijola and T. Mattila, "Modeling of nonlinear micromechanical resonators and their simulation with the harmonic-balance method," *Int. J. RF Microwave Computer-Aided Eng.*, vol. 11, no. 5, pp. 310–321, Sep. 2001.

[15] European Telecommunications Standards Institute (ETSI), "GSM global system for mobile communications, 3GPP TS 05.01/05.05," 2003.

[16] T. Ranta, J. Ellä, and H. Pohjonen, "Antenna switch linearity requirements for GSM/WCDMA mobile phone front-ends," in *8th Eur. Conf. Wireless Technol.*, Paris, France, 3–4 Oct. 2005, pp. 23–26.

[17] S.-S. Li, Y.-W. Lin, Y. Xie, Z. Ren, and C. T.-C. Nguyen, "Micromechanical 'hollow-disk' ring resonators," in *Tech. Dig. Int. IEEE Microelectromechanical Syst. Conf.*, Maastricht, The Netherlands, 25–29 Jan. 2001, pp. 821–824.

[18] T. Mattila, J. Kiihamäki, T. Lamminmäki, O. Jaakkola, P. Rantakari, A. Oja, H. Seppä, H. Kattelus, and I. Tittonen, "12 MHz micromechanical bulk acoustic mode oscillator," *Sens. Actuators A*, vol. 101, no. 1-2, pp. 1–9, Sep. 2002.

[19] S. A. Bhave and R. T. Howe, "Internal electrostatic transduction for bulk-mode MEMS resonators," in *Solid State Sensor, Actuator and Microsystems Workshop (Hilton Head 2004)*, Hilton Head Island, SC, 6–10 June 2004, pp. 59–60.

Ari T. Alastalo received the M.Sc. degree in technical physics in 1997 from Helsinki University of Technology (HUT). From 1996 to 1998 he was an assistant at HUT working in the area of magnetic quantum impurities. From 1998 to 2001 he was with Nokia Research Center carrying out research of radio propagation, RF architectures, baseband algorithms and protocols for adaptive-antenna systems. Since 2002 he has been a Research Scientist at VTT. His present research focuses on RF MEMS.

Ville Kaajakari received his M.S. and Ph.D. degrees in electrical and computer engineering from University of Wisconsin-Madison in 2001 and 2002, respectively. He is currently Senior Research Scientist at VTT Information Technology, Finland, where his research interest is RF-MEMS.